Resource

Chemistry & Biology

Quantitative Analysis of Proteome and Lipidome Dynamics Reveals Functional Regulation of Global Lipid Metabolism

Graphical Abstract

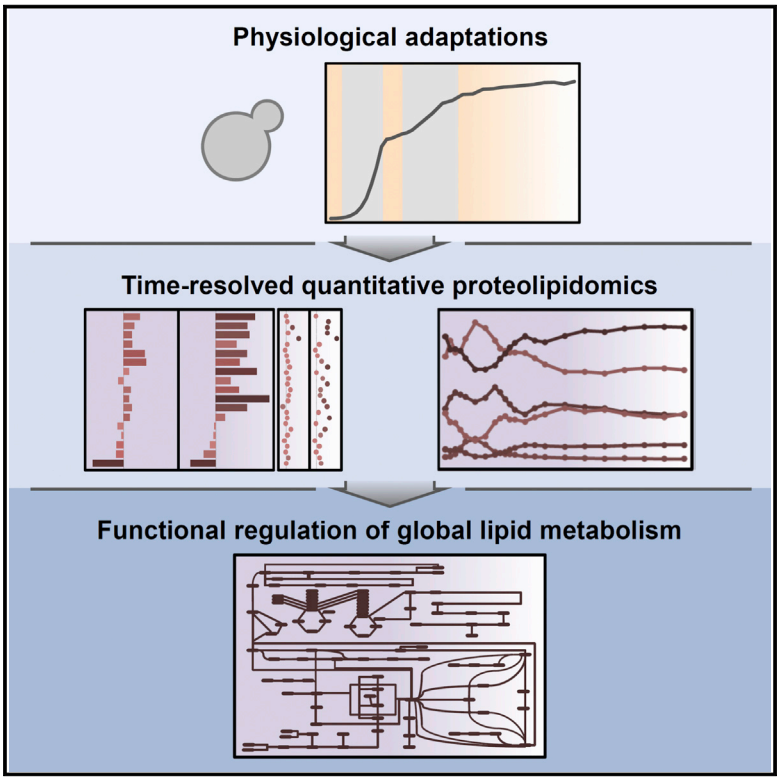

Authors

Albert Casanovas, Richard R. Sprenger, ..., Ole N. Jensen, Christer S. Ejsing

Correspondence

cse@bmb.sdu.dk

In Brief

Casanovas et al. present a proteolipidomics platform for a comprehensive and quantitative time-resolved analysis of the yeast proteome and lipidome. Application of this platform demonstrates that lipid metabolism is regulated at the global scale and coordinated with remodeling of cellular architecture and processes during physiological adaptations.

Highlights

- Time-resolved quantitative analysis of 3,673 proteins and 223 lipid species in yeast
- Physiological regulation of global lipid metabolism
- Lipid droplets undergo differential turnover of triacylglycerols and sterol esters
- Endogenous modulation of fatty acid unsaturation regulates protein expression

Casanovas et al., 2015, Chemistry & Biology 22, 412–425
March 19, 2015
http://dx.doi.org/10.1016/j.chembiol.2015.02.007

CellPress

CellPress

Chemistry & Biology
Resource

Quantitative Analysis of Proteome and Lipidome Dynamics Reveals Functional Regulation of Global Lipid Metabolism

Albert Casanovas,[1] Richard R. Sprenger,[1] Kirill Tarasov,[2] David E. Ruckerbauer,[3,4] Hans Kristian Hannibal-Bach,[1] Jürgen Zanghellini,[3,4] Ole N. Jensen,[1] and Christer S. Ejsing[1,*]
[1]Department of Biochemistry and Molecular Biology, VILLUM Center for Bioanalytical Sciences, University of Southern Denmark, 5230 Odense, Denmark
[2]Département de Biochimie, Université de Montréal, Succ. Centre-Ville, 6128 Montreal, Quebec H3C 3J7, Canada
[3]Austrian Centre of Industrial Biotechnology, 1190 Vienna, Austria
[4]Department of Biotechnology, University of Natural Resources and Life Sciences, 1190 Vienna, Austria
*Correspondence: cse@bmb.sdu.dk
http://dx.doi.org/10.1016/j.chembiol.2015.02.007

SUMMARY

Elucidating how and to what extent lipid metabolism is remodeled under changing conditions is essential for understanding cellular physiology. Here, we analyzed proteome and lipidome dynamics to investigate how regulation of lipid metabolism at the global scale supports remodeling of cellular architecture and processes during physiological adaptations in yeast. Our results reveal that activation of cardiolipin synthesis and remodeling supports mitochondrial biogenesis in the transition from fermentative to respiratory metabolism, that down-regulation of de novo sterol synthesis machinery prompts differential turnover of lipid droplet-associated triacylglycerols and sterol esters during respiratory growth, that sphingolipid metabolism is regulated in a previously unrecognized growth stage-specific manner, and that endogenous synthesis of unsaturated fatty acids constitutes an in vivo upstream activator of peroxisomal biogenesis, via the heterodimeric Oaf1/Pip2 transcription factor. Our work demonstrates the pivotal role of lipid metabolism in adaptive processes and provides a resource to investigate its regulation at the cellular level.

INTRODUCTION

Lipids are essential constituents of all living organisms with crucial roles in membrane structure and dynamics, energy homeostasis, and signal transduction (Shevchenko and Simons, 2010). The full lipid complement (i.e., lipidome) of eukaryotic cells comprises several hundred molecular lipid species produced by a metabolic network that interconnects the metabolism of fatty acids, glycerophospholipids, glycerolipids, sphingolipids, and sterol lipids (Ejsing et al., 2009; Gaspar et al., 2011; Rajakumari et al., 2010). This network enables modulation of the lipidome to support remodeling of cellular processes and architecture during physiological adaptations. Previous research has characterized most components of the lipid metabolic network but has provided little insight into the physiological regulation of lipid metabolism on the global scale. Dysfunctional regulation of lipid metabolism and homeostasis causes cellular lipotoxicity, impairs cellular processes and contributes to the pathogenesis of disorders such as obesity, atherosclerosis, and neurodegeneration (Wymann and Schneiter, 2008). Understanding the physiological regulation of global lipid metabolism warrants quantitative data that capture the dynamics of both lipid species and the proteins that operate the lipid metabolic network and cellular processes undergoing adaptation.

Insights into the dynamic regulation of metabolism have been provided by time series analysis combining proteomics, metabolomics, and other "omics" technologies (Buescher et al., 2012; Zampar et al., 2013). The functional analysis of global lipid metabolism and its regulation is supported by recent advances in lipidomics technology (Carvalho et al., 2012; Dennis et al., 2010; Ejsing et al., 2009). So far, studies combining lipidomics and proteomics are scarce and have been restricted to either analyzing steady-state conditions (Grillitsch et al., 2011; Thibault et al., 2012) or monitoring the dynamics of a single lipid metabolic pathway (Sabido et al., 2012), thus precluding assessment of the dynamic regulation of global lipid metabolism and its physiological impact at the system level.

Targeted proteomics based on selected reaction monitoring (SRM) has been successfully applied to quantify the changes in abundance of a set of enzymes operating in central carbon metabolism (Picotti et al., 2009; Zampar et al., 2013). This strategy, however, is of limited efficacy for deciphering the interplay between metabolic regulation and coordinated restructuring of cellular architecture and processes. Recent advances in shotgun (i.e., non-targeted) proteomics have maximized the scope of proteomic approaches enabling the quantification of virtually complete proteomes in tractable model organisms such as yeast (Mann et al., 2013). Stable isotope labeling by amino acids in cell culture (SILAC) has been applied for comprehensive quantification of the yeast proteome (de Godoy et al., 2008) but this approach uses a defined nutrient composition that can adversely affect the dynamics of metabolism (Hanscho et al., 2012). By contrast, label-free quantification methods are suitable for any

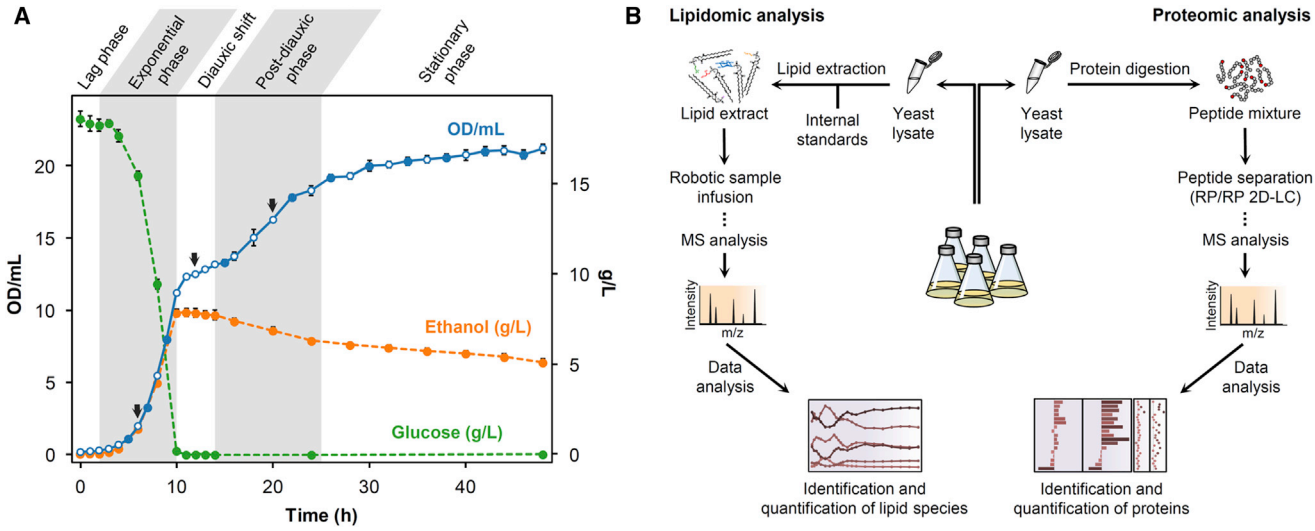

Figure 1. Strategy for Quantitative Proteomic and Lipidomic Analysis along the Growth Profile of *S. cerevisiae*

(A) Cell density (OD/ml), and extracellular glucose and ethanol concentrations. The results are expressed as the mean ± SD of five biological replicates. Time points for proteomic and lipidomic analysis are indicated with arrows and open blue circles, respectively. Growth stages are indicated at the top. Shaded areas correspond to phases of proliferation. See also Table S4 and File S3.

(B) Outline of the proteolipidomic platform. Samples were processed in parallel for quantitative proteomic and lipidomic analysis. 2D-LC, two-dimensional liquid chromatography; MS, mass spectrometry; RP, reversed phase.

experimental condition (Neilson et al., 2011) and have been successfully employed to quantify proteins on a global scale (Marguerat et al., 2012).

Here, we combine comprehensive quantitative proteomics and lipidomics (which we term proteolipidomics) to analyze how global lipid metabolism and cellular processes are dynamically co-regulated during physiological adaptations. For this, we performed a time-resolved proteomic and lipidomic analysis of the *Saccharomyces cerevisiae* growth profile covering conserved metabolic programs and physiological adaptations. This experimental framework enables the comparison between fermentative and respiratory metabolism as well as between proliferating and quiescent cells in a physiological context. In higher eukaryotes, the ability to alternate between quiescence and proliferation regulates development and tissue homeostasis (Coller, 2011), whereas the switch between metabolic programs impinges on cell growth and is central to proliferative diseases such as cancer (Locasale and Cantley, 2011).

Our results reveal system-wide remodeling of the cell proteome and lipidome that interlink the regulation of global lipid metabolism with the functional restructuring of cellular architecture and processes. In particular, we demonstrate that the lipid enzymatic machinery is reprogrammed to support cardiolipin (CL) synthesis and remodeling for mitochondrial function, that lipid droplet-associated triacylglycerol (TG) and sterol ester (SE) undergo distinct cycles of storage and mobilization, that sphingolipid composition is dynamically adjusted in a growth stage-specific manner, and that modulation of endogenous fatty acid unsaturation participates in the control of peroxisomal biogenesis in vivo. This study provides a quantitative resource for future work toward a systems-level understanding of the regulation and function of global lipid metabolism.

RESULTS AND DISCUSSION

Experimental Framework for Monitoring Physiological Regulation of Metabolism

To uncover the regulation of global lipid metabolism during physiological adaptations, we quantified the proteome and lipidome dynamics along the growth profile of yeast (Figure 1). For this, *S. cerevisiae* cells were sampled throughout 48 hr of growth in batch culture in glucose-based rich medium (YPD), covering a series of growth stages with distinct metabolic hallmarks and physiological adaptations. We monitored cell density and the extracellular concentration of glucose and ethanol to define the temporal boundaries between these growth stages (Figure 1A). Initially, cells adjust their metabolism during a temporary lag phase to meet the demands of the subsequent proliferative exponential phase, when growth is fueled by fermentation of glucose to ethanol. Upon glucose depletion, cells enter a transient quiescent phase, the diauxic shift, where metabolism is reprogrammed to support growth in the post-diauxic phase by using cellular respiration of ethanol and other substrates (e.g., fatty acids, see Supplemental Discussion). Finally, cells enter the quiescent stationary phase as growth ceases upon depletion of a limiting nutrient (not carbon) (Werner-Washburne et al., 1993). The range of distinct growth stages makes this experimental framework well suited for studying the regulation of metabolic networks in the context of physiological adaptations.

Proteome Quantification at Different Growth Stages

To characterize the remodeling of cellular processes and pathways during the transition from fermentation to respiration, we quantified the proteome in the exponential phase (6 hr), the diauxic shift (12 hr), and the post-diauxic phase (20 hr) in five

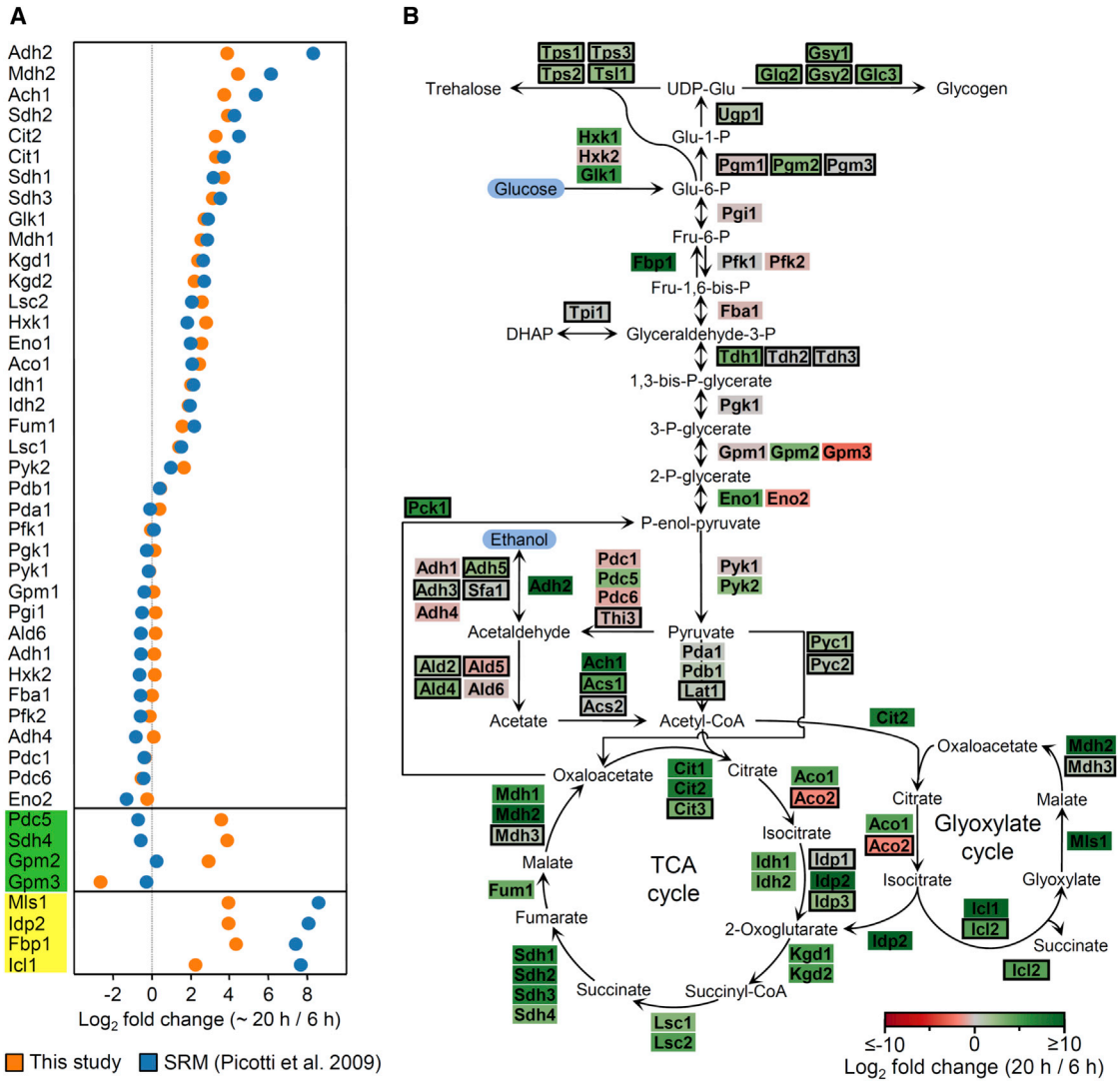

Figure 2. Benchmarking the Quantitative Proteomics Strategy for Metabolic Studies

(A) Fold changes of 45 enzymes in central carbon metabolism compared with a similar study using SRM (Picotti et al., 2009). The comparison uses time points selected from the SRM study (ratio 19.8 hr/6.5 hr) that best match our time points (ratio 20 hr/6 hr). Data represent the mean fold change of three (SRM study) or five (this study) biological replicates. Discordant proteins are highlighted in green (see Figure S2 for comparison with other reference data). Proteins highlighted in yellow were quantified in the SRM study using noise as the abundance at time point 6.5 hr, and are therefore less suitable for fold change comparison.

(B) Reprogramming of the central carbon metabolic network. Fold changes (ratio 20 hr/6 hr) of proteins quantified in this study are indicated by color. Proteins quantified in this study but not in the SRM study are framed.

See also Figures S1, S2, and Table S1.

biological replicates (Figure 1A). We quantified 3,673 proteins (Table S1) with an average coefficient of variation of 15%, placing this dataset among the most comprehensive and reproducible yeast proteomes reported in a comparative study (Figure S1). To benchmark the proteomic strategy, we first compared our results with a similar study where only 45 enzymes in the central carbon metabolism were monitored by SRM (Picotti et al., 2009), the gold-standard method in quantitative proteomics (Domon and Aebersold, 2010). Our data for these 45 proteins closely mirror that of the previous study (Figure 2A). A few discordant proteins between both datasets showed a better concordance between our results and other reference data (Figure S2), demonstrating the accuracy of our proteome dataset.

Next, we assessed the efficacy of the proteomic analysis for pinpointing regulated proteins in metabolic pathways. To this end, we compared the abundance of enzymes in the central carbon metabolism between fermentative (6 hr) and respiratory (20 hr) growth (Figure 2B). Our proteomic strategy afforded the monitoring of an additional 35 enzymes in the central carbon metabolism compared with the SRM study (Picotti et al., 2009). Our results show that the exhaustion of glucose prompts (i) degradation of ethanol to acetyl-coenzyme A (acetyl-CoA) via increased levels of Adh2, Ald2, Ald4, Ach1, and Acs1;

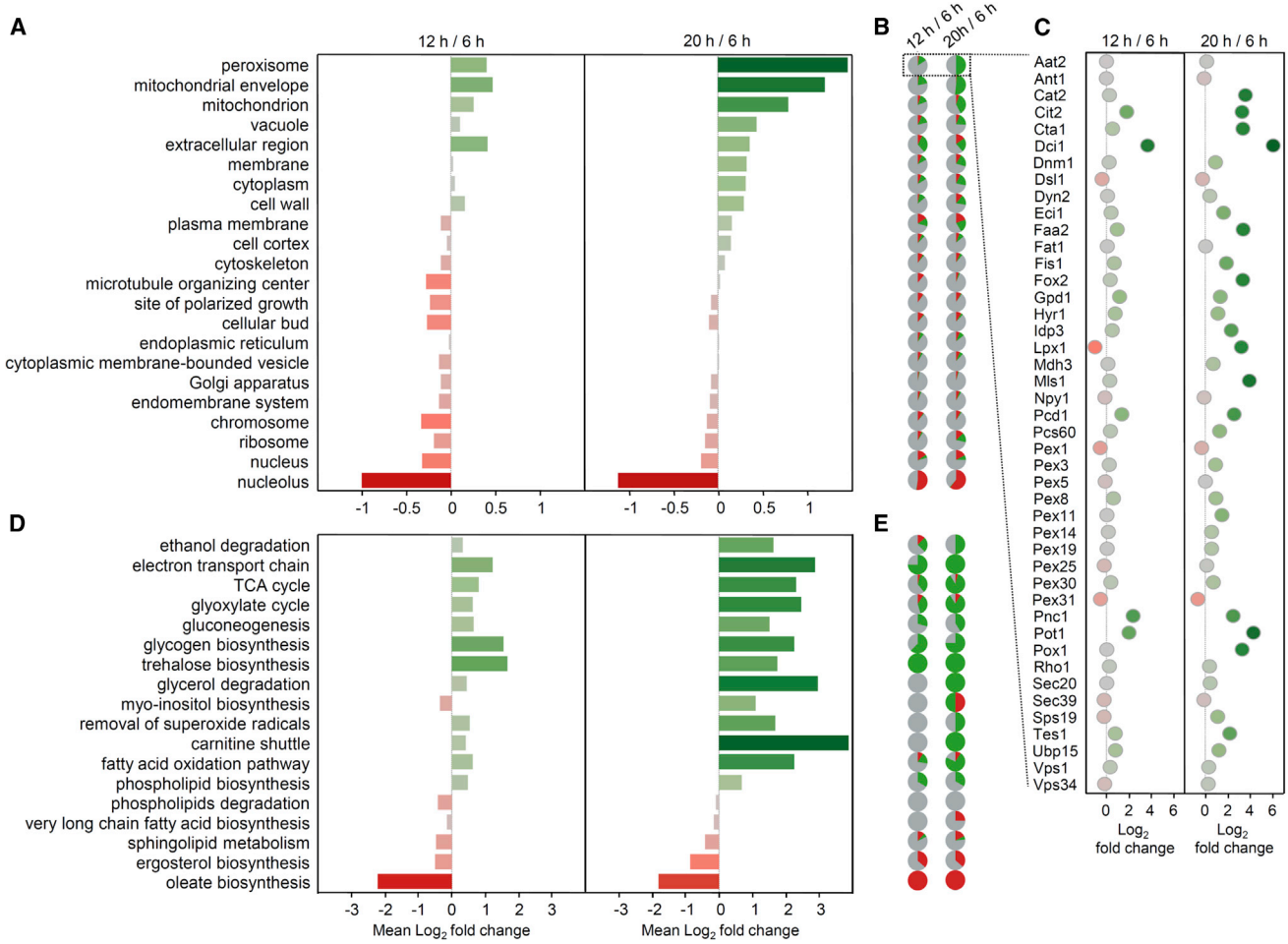

Figure 3. Metabolic Transitioning Mediates Remodeling of Cellular Architecture and Processes

(A) Mean fold change of proteins associated with indicated cellular components.

(B) Proportion of proteins up-regulated ≥2-fold (green), down-regulated ≥2-fold (red), and changing <2-fold (gray) within each cellular component.

(C) Fold changes of peroxisomal proteins (mean of five biological replicates) are shown as a representative example. Fold changes of individual proteins within each category can be accessed in File S1.

(D) Mean fold change of proteins associated with indicated biochemical pathways.

(E) Proportion of proteins up-regulated ≥2-fold (green), down-regulated ≥2-fold (red), and changing <2-fold (gray) within each biochemical pathway.

See also Table S1.

(ii) induction of enzymes in the tricarboxylic acid (TCA) cycle and the glyoxylate cycle; (iii) up-regulation of the gluconeogenic enzymes Pck1 and Fbp1; and (iv) up-regulation of the enzymatic machinery for synthesis of storage carbohydrates. These data are consistent with current knowledge and provide a more extensive characterization of protein expression and the reprogramming of central carbon metabolism compared with previous proteomic studies (Picotti et al., 2009). We conclude that the proteome dataset is comprehensive, accurate, and reproducible, and that it affords interrogating the dynamics of metabolic networks at the molecular level. We note that although our proteomic strategy determines changes in protein abundance, it does not allow monitoring other levels of regulation of protein function such as post-translational modifications and subcellular localization, which can also affect the regulation of metabolism.

Proteome Remodeling Modulates Organelle Dynamics and Cellular Metabolism

The transition from fermentation to respiration entails extensive remodeling of the yeast proteome with 3,105 proteins showing significant differences in abundance (ANOVA *f* value and *t* test *p* value <0.05). To assess which physiological processes are modulated, we sorted proteins based on gene ontology (GO) categories for cellular components and biochemical pathway annotation, and determined the mean fold change within each structural or functional category (Figure 3; File S1). Changes related to cellular components (Figures 3A–3C) show (i) increased levels of mitochondrial proteins consistent with the increase of mitochondrial content when cells are transferred from a fermentable to a non-fermentable carbon source (Egner et al., 2002); (ii) an increase in levels of peroxisomal proteins consistent with peroxisome proliferation in the

post-diauxic phase (Lefevre et al., 2013); and (iii) a decrease in nucleolar and ribosomal proteins showing a down-regulation of protein synthesis, with the exception of mitochondrial ribosomal proteins which are up-regulated in the post-diauxic phase (Figure 3B). Assessing co-regulated biochemical pathways (Figures 3D and 3E) confirms the aforementioned induction of ethanol degradation, the TCA cycle, the glyoxylate cycle, and gluconeogenesis, and uncovered other processes activated in the post-diauxic phase including (i) the oxidation of fatty acids, (ii) the related carnitine shuttle and removal of superoxide radicals, (iii) the degradation of glycerol, and (iv) the synthesis of the lipid precursor inositol. Conversely, the protein machinery implicated in sterol metabolism, sphingolipid metabolism, and the synthesis of oleic acid (C18:1) was down-regulated (Figure 3D). These results demonstrate that the diauxic shift and post-diauxic phase have wide-ranging implications for cellular metabolism beyond the well-known remodeling of central carbon metabolism, and illustrate the efficacy of the non-targeted proteomic strategy for mapping co-regulated processes and pathways. In particular, the results indicate coordinated regulation of lipid metabolic processes and organelle biogenesis during the diauxic shift.

Physiological Adaptation Mediates Reprogramming of the Lipid Metabolic Network

To study the changes in lipid metabolism at the cellular level, we constructed a map of the yeast lipid metabolic network that comprises 138 proteins and depicts the interdependent pathways of fatty acid, glycerophospholipid, glycerolipid, sphingolipid, and sterol lipid metabolism (Figure 4). We projected the changes in protein abundance onto the network to evaluate the reprogramming of lipid metabolism (Figure 4). Overall, 85% of the proteins in the lipid metabolic network were quantified, yielding a coverage similar to that of other yeast metabolic networks analyzed by targeted proteomics (Costenoble et al., 2011). This analysis shows that 96 proteins in the lipid metabolic network change significantly, and that most changes occur during the diauxic shift and persist in the post-diauxic phase (Figure S3). In particular, the physiological adaptation entails (i) a decrease in expression of the fatty acid desaturase Ole1 and the fatty acid elongase Sur4 (Figure 4-A1); (ii) differential expression of the fatty acyl-CoA synthetases Faa1, Faa2, Faa3, and Faa4 (Figure 4-A1) indicating distinct roles of these enzymes in the adaptive processes; (iii) down-regulation of several ergosterol biosynthetic enzymes (Figure 4-C1); (iv) changes in the levels of glycerophospholipid enzymes (e.g., increase in Opi3 and Cki1 levels; Figure 4-C3); (v) reduced levels of the sphingolipid enzymes Lcb1 and Tsc10 (Figure 4-A3), and a concomitant increase of the ceramidase Ydc1 (Figure 4-B3); and (vi) differential expression of isoenzymes involved in the synthesis and turnover of the storage lipids TG (Figure 4-C3) and SE (Figures 4-B1 and 4-B2). We conclude that the switch from fermentative to respiratory metabolism entails extensive reprogramming of the lipid metabolic network.

Lipidome Dynamics during Physiological Adaptation of Cellular Metabolism

For a comprehensive assessment of the changes in cellular lipid composition accompanying the proteome changes, we executed a quantitative lipidomic analysis across 22 time points covering all growth stages (Figure 1A). We quantified 223 lipid species (annotated by sum composition, see Experimental Procedures) encompassing 21 lipid classes. The levels of 19 lipid classes (Figure 5) and the relative abundance of 221 lipid species (Figure 6; Figure S5) change significantly along the growth profile (ANOVA f value and t test p value <0.05, Tables S2 and S3). This result demonstrates extensive modulation of the lipidome at a scale beyond what can be discerned analyzing only the protein complement of the cell. In particular, the ratio between storage and membrane lipids fluctuates markedly across all growth stages, showing accumulation of TG and SE lipids when cells enter quiescent phases and mobilization during proliferation when membrane lipids are required for secretory traffic and expansion of the plasma membrane (Figure 5A). Specific glycerophospholipid classes (i.e., CL and phosphatidylcholine [PC]) increase after the diauxic shift (Figures 5B and 5C) corroborating the observed up-regulation of the corresponding enzymatic machinery (Figures 4-B2 and 4-C3). Interestingly, the total levels of sphingolipids (Figure S4) and sterols (Figure 5F) remain stable across all growth stages despite the down-regulation of their de novo biosynthetic machinery (Figure 4-C1), indicating that additional mechanisms control their abundance. Taken together, these findings highlight the complementarity of the lipidomics and proteomics data and show their utility as a resource for exploring the functional reprogramming of global lipid metabolism and its co-regulation with adaptive cellular processes.

Synthesis and Functional Remodeling of CL during Mitochondrial Biogenesis

Mitochondrial biogenesis is induced to support cellular respiration (Egner et al., 2002). CL is a mitochondrial lipid class required for mitochondrial morphogenesis and optimal function of the electron transport chain and ATP synthase (Paradies et al., 2014). Higher CL levels and CL synthase activity have been shown when cells are grown on a non-fermentable carbon source compared with a fermentable carbon source (Tuller et al., 1998). Accordingly, during the diauxic shift and the post-diauxic phase, CL levels increase (Figure 5B) providing additional evidence for the biogenesis of mitochondria as deduced from the proteomic data (Figure 3A). Previous analysis under steady-state conditions have shown that the four acyl chains of CL species comprise mainly palmitoleoyl (C16:1) and oleoyl (C18:1) moieties incorporated primarily by post-synthetic acyl chain remodeling (Schlame, 2013). CL remodeling occurs through the coordinated action of the phospholipase Cld1, which removes an acyl chain producing monolysocardiolipin (MLCL), and the transacylase Taz1, which incorporates C16:1 and C18:1 yielding CL species with up to four monounsaturated fatty acid (MUFA) moieties. Up-regulation of Taz1 (Figure 4-B2) during the diauxic shift and the post-diauxic phase implies activation of CL remodeling. Accordingly, as cells transit from the exponential to the post-diauxic phase, the pool of CL species undergoes a systematic increase in the proportion of MUFA chains reaching a plateau where ~90% of all species comprise four MUFAs (Figures 6A, 6E, and S6). Consistent with the activation of CL remodeling, MLCL levels are also increased after the exponential phase (Figure 5B) and MLCL species show an increase in the proportion of MUFA chains parallel to that of CL species (Figures 6B,

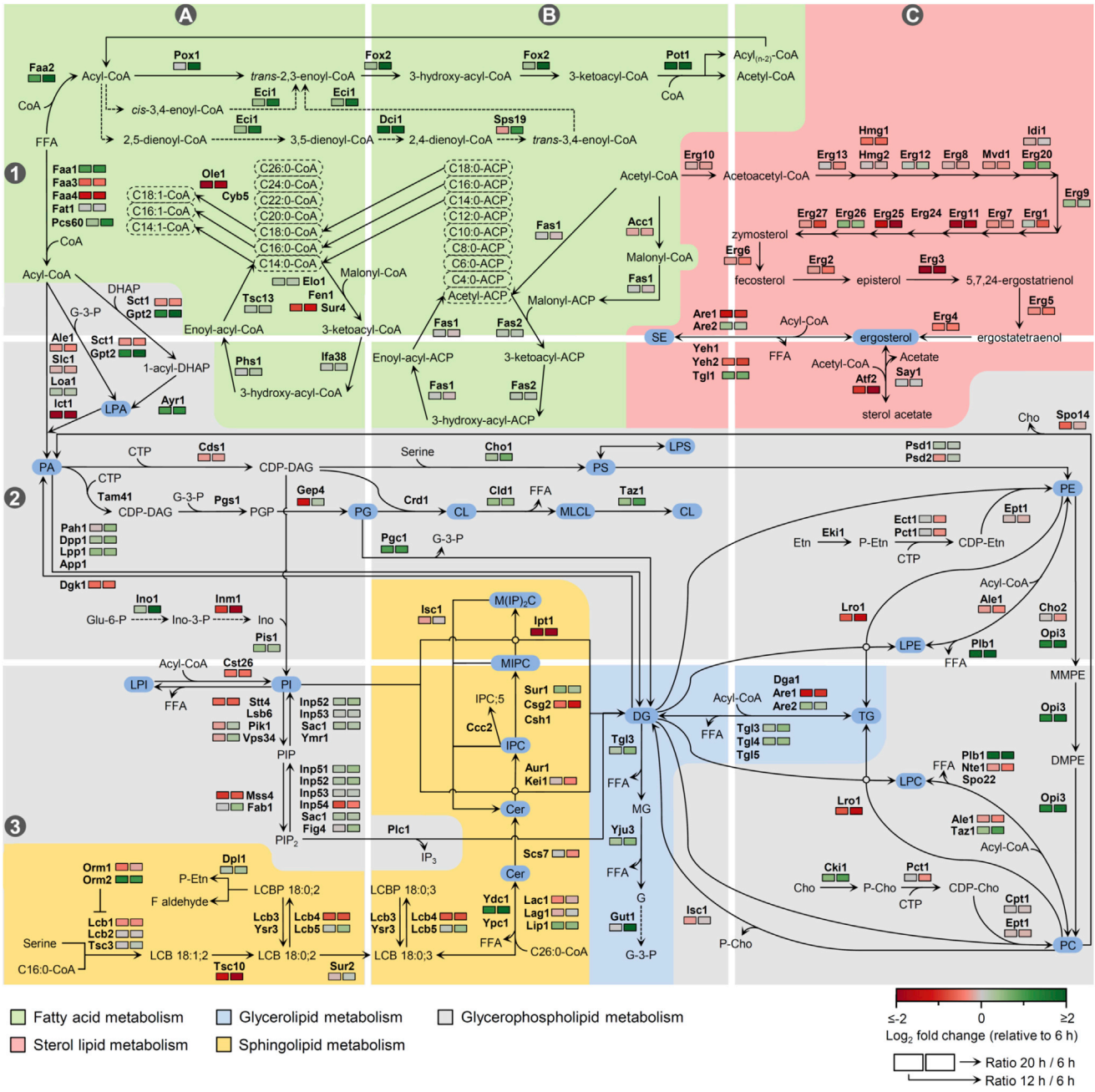

Figure 4. Functional Reprogramming of the Lipid Metabolic Network during the Diauxic Shift and the Post-Diauxic Phase

The yeast lipid metabolic network was compiled from the *Saccharomyces* Genome Database and references therein. Fold changes of proteins quantified (relative to time point 6 hr) are indicated by color (mean of five biological replicates). Lipids monitored are highlighted in blue. Background colors indicate different lipid metabolic pathways. A coordinate system is used to reference proteins discussed in the text. See also Figure S3 and Table S1.

6F, and S6). These results demonstrate in vivo CL remodeling during physiological induction of mitochondrial biogenesis. The importance of CL remodeling is underscored by the fact that mutations in the taffazzin gene, the human ortholog of *TAZ1* (Gu et al., 2004), cause Barth syndrome (Bione et al., 1996). Our results show that the experimental framework applied in our study can serve as a new testing ground for mechanistic studies of CL acyl chain remodeling and its physiological regulation.

Lipidome Dynamics Reveal Extensive Reprogramming of Glycerophospholipid Metabolism

Glycerophospholipids are major constituents of cellular membranes with pivotal roles in secretory trafficking, organelle identity, and anchoring of membrane proteins (van Meer et al., 2008). Assessment of glycerophospholipid composition demonstrated extensive dynamics across all growth phases (Figures 5C and 5D). Glycerophospholipid levels increase

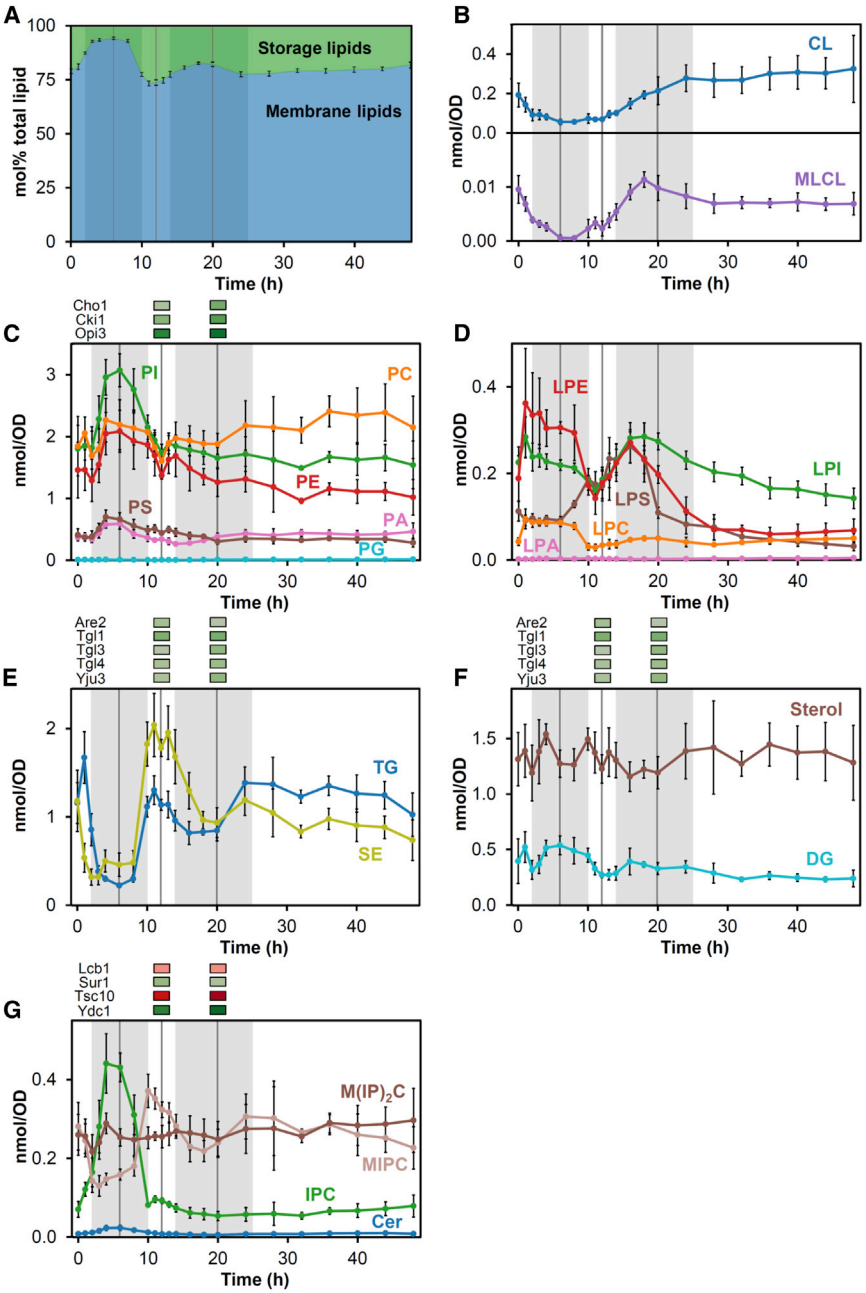

Figure 5. Modulation of Lipid Class Composition along the Growth Profile of *S. cerevisiae*

(A) Temporal dynamics of storage (TG and SE) and membrane lipids. The results are expressed as the mean ± SD of five biological replicates. Statistical comparisons by repeated measures ANOVA and post hoc paired *t* test (see Table S2). Vertical lines indicate the time points selected for proteomic analysis. Shaded areas correspond to phases of proliferation.

(B–G) Temporal profiles of 21 lipid classes. The results are expressed as the mean ± SD of five biological replicates. Statistical comparisons as in (A) (see Table S2). Fold changes (12 hr/6 hr and 20 hr/6 hr) of proteins discussed in the text are indicated by color (as in Figure 4) at the top of the related panels. Vertical lines and shaded areas as in (A). Cer, ceramide; CL, cardiolipin; DG, diacylglycerol; IPC, inositolphosphoceramide; LPA, lysophosphatidic acid; LPC, lysophosphatidylcholine; LPE, lysophosphatidylethanolamine; LPI, lysophosphatidylinositol; LPS, lysophosphatidylserine; $M(IP)_2C$, mannosyl-diinositolphosphoceramide; MIPC, mannosyl-inositolphosphoceramide; MLCL, monolysocardiolipin; PA, phosphatidic acid; PC, phosphatidylcholine; PE, phosphatidylethanolamine; PG, phosphatidylglycerol; PI, phosphatidylinositol; PS, phosphatidylserine; SE, sterol ester; TG, triacylglycerol.

See also Figure S4, Table S2, and File S2.

during cell proliferation as secretory traffic drives membrane expansion and cell division (Figure S4). This increase in glycerophospholipid levels during the exponential phase is primarily caused by an increase in phosphatidylinositol (PI) and phosphatidylethanolamine (PE) levels (Figure 5C). Notably, the glycerophospholipid composition of exponential phase cells is consistent with previous studies using shotgun lipidomics (Fairn et al., 2011; Klose et al., 2012) but contrasts with other studies using classical approaches (i.e., thin-layer chromatography) (Le Guedard et al., 2009). Following the diauxic shift, there is a gradual elevation in PC levels. This increase in PC is supported by up-regulation of enzymes synthesizing PC via the CDP-choline pathway (Cki1) and the PE methylation pathway (Opi3) (Figure 4-C3). Moreover, the up-regulation of the phosphatidylserine (PS) synthase Cho1 (Figure 4-B2) and the concomitant decrease in PS and PE levels (Figure 5C), suggest that the increase in PC is derived in part from sequential conversion of PS. In addition, the level of phospholipase Plb1, which participates in the remodeling of PC species, is also increased in the diauxic shift and the post-diauxic phase (Figure 4-C3), and coincides with systematic changes in the composition of PC and lysophosphatidylcholine species (Figures 6K and 6L) demonstrating activation of PC remodeling.

Moreover, our results provide a new perspective on transcriptional regulation of glycerophospholipid metabolism. The expression of a subset of enzymes involved in glycerophospholipid synthesis is controlled by the transcriptional regulators Ino2, Ino4, and Opi1 (Henry et al., 2012). The regulated genes include the above-mentioned *OPI3*, *CKI1* and *CHO1*, and *INO1* encoding inositol-3-phosphate synthase (Figure 4-A2). These enzymes show increased expression during the post-diauxic phase. The current model of the transcriptional regulation posits that high phosphatidic acid (PA) levels sequester Opi1 in the ER membrane allowing the heterodimeric Ino2-Ino4 transcription factor to activate gene expression (Henry et al., 2012). Conversely, upon reduction in PA levels, Opi1 is released from the ER, enters

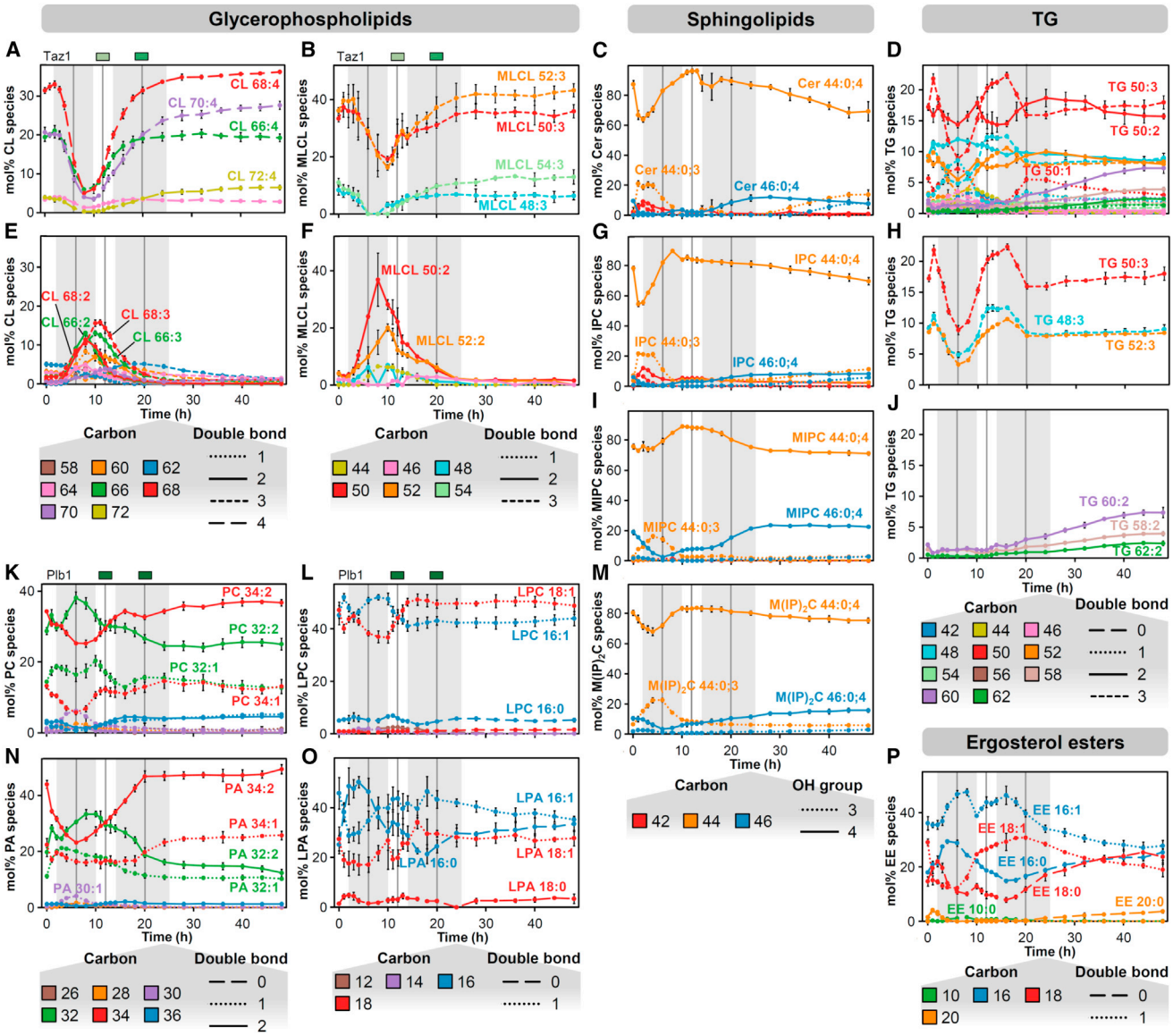

Figure 6. Modulation of Lipid Species Composition along the Growth Profile of *S. cerevisiae*

223 lipid species were quantified.

(A–P) Temporal profiles of lipid species within each lipid class for selected lipid classes. Lipid species are annotated by sum composition (see Experimental Procedures). The total number of carbon atoms, double bonds, and hydroxyl groups in the lipid molecule are depicted using distinct color and line format. The most abundant lipid species are annotated. Low abundant lipid species are omitted for clarity. The results are expressed as the mean ± SD of five biological replicates. Statistical comparisons by repeated measures ANOVA and post hoc paired *t* test (see Table S3). Vertical lines indicate the time points selected for proteomic analysis. Shaded areas correspond to phases of proliferation. Fold changes (12 hr/6 hr and 20 hr/6 hr) of proteins discussed in the text are indicated by color (as in Figure 4) at the top of the related panels. (A) CL species with 4 double bonds; (B) MLCL species with 3 double bonds; (C) Cer species; (D) TG species; (E) CL species with ≤3 double bonds; (F) MLCL species with ≤2 double bonds; (G) IPC species; (H) selected TG species with 3 double bonds; (I) MIPC species; (J) selected TG species with 2 double bonds and a carbon index ≥58; (K) PC species; (L) LPC species; (M) $M(IP)_2C$ species; (N) PA species; (O) LPA species; (P) ergosterol ester (EE) species.

See also Figures S5 and S6, Table S3, and File S2.

the nucleus, binds Ino2, and attenuates gene expression. Our results show that high PA levels occur primarily during the exponential phase when PI synthesis is elevated (Figure 5C). This finding contrasts the model of transcriptional regulation which predicts increased PC synthesis, attributed to the high PA levels and, hence, expected expression of PC biosynthetic enzymes. Notably, our results support the model for transcriptional regulation during the post-diauxic phase when the majority of the expected enzymes are up-regulated, although only a minor increase in PA levels is observed (Figure 5C). Instead a pronounced alteration of the PA species profile occurs (Figure 6N) suggesting that distinct molecular PA species play different roles

in the transcriptional program of glycerophospholipid metabolism. Furthermore, our data indicate that a more extensive regulatory network fine-tunes the expression level of lipid metabolic enzymes and that this network is intertwined with the processes orchestrating physiological adaptations.

Growth Stage-Specific Modulation of Sphingolipid Metabolism

Sphingolipids have essential roles in membrane trafficking and cell signaling (Dickson, 2008). Inspection of the sphingolipidome shows that the total sphingolipid content remains relatively stable across all growth phases (Figure S4) while levels of sphingolipid classes and species show distinct temporal profiles. Specifically, increase of ceramide (Cer) and inositolphosphoceramide (IPC) levels demonstrates activation of sphingolipid biosynthesis during the exponential phase (Figure 5G). Moreover, sphingolipid species with three hydroxyl groups are increased in the early exponential phase and progressively converted to more common species featuring four hydroxyl groups (Figures 6C, 6G, 6I, and 6M). The sphingolipid biosynthesis is attenuated in the late exponential phase and diauxic shift coinciding with an elevated conversion of IPC to mannosyl-inositolphosphoceramide (MIPC). This metabolic transition is likely driven by the down-regulation of sphingolipid biosynthetic enzymes including Lcb1 and the reductase Tsc10 (Figure 4-A3) and up-regulation of the ceramidase Ydc1 (Figure 4-B3), which collectively can mediate the reduction of Cer levels in the lipidome (Figure 5G). In addition, up-regulation of the catalytic subunit of the MIPC synthase Sur1 (Figure 4-B3) supports the observed increase in MIPC levels. Notably, $M(IP)_2C$ levels remain stable across all growth stages indicating tight control of its abundance (Figure 5G). Interestingly, the recently discovered negative regulators of sphingolipid synthesis Orm1 and Orm2 (Breslow et al., 2010) are differentially regulated (Figure 4-A3), suggesting growth stage-specific functions for each Orm protein. Our findings demonstrate modulation of the sphingolipidome according to the physiological program of the cell, and provide a new experimental framework for investigating the regulation of sphingolipid metabolism and the influence of the related TORC2 signaling machinery, Rom2, Ypk1, the Orm proteins, and the putative sensor Slm1 (Aguilar et al., 2010; Berchtold et al., 2012; Roelants et al., 2011).

Lipid Droplets Undergo Distinct Cycles of Storage Lipid Accumulation and Mobilization

TG and SE are storage lipids deposited in and mobilized from lipid droplets dependent on physiological requirements (Kohlwein et al., 2013). Lipid droplets buffer lipid substrates for membrane synthesis and energy production via β-oxidation. The temporal profiles of TG and SE lipids demonstrate high plasticity of lipid droplets in vivo (Figure 5E). Interestingly, storage lipids undergo two distinct cycles of mobilization and accumulation prompted by active growth and quiescence, respectively (Figure 5A). Accumulated TG and SE lipids are initially mobilized as cells enter the lag phase and re-synthesized as cells transit into the diauxic shift. Under these conditions, TG and SE lipids are present in similar amounts as previously reported (Kohlwein et al., 2013) and exhibit parallel temporal profiles. Conversely, as cells enter the post-diauxic growth phase, TG and SE are mobilized but exhibit distinct dynamics. Assessing the enzyme machinery directing the mobilization shows high expression of the lipases Tgl3, Tgl4 (Figure 4-C3), and Tgl1 (Figure 4-B2) during the post-diauxic phase, suggesting that these enzymes mediate the hydrolysis of TG and SE. Similarly, the lipase Yju3, which converts monoacylglycerol to fatty acid and glycerol, is also up-regulated (Figure 4-B3), indicating that at least part of the TG pool can be fully hydrolyzed to direct fatty acids into energy production. Accordingly, the main machinery for peroxisomal β-oxidation, comprising Pox1, Fox2, Pot1, and the acyl-CoA synthetase Faa2, is also up-regulated (Figures 4-A1 and 4-B1). The activation of β-oxidation coinciding with the mobilization of storage lipids was further substantiated by flux balance analysis, which shows that growth upon exit from the diauxic shift is supported by channeling of fatty acids toward β-oxidation (see Supplemental Discussion, Table S4, and File S3).

As cells approach the stationary phase, TG is re-synthesized, whereas the SE pool is kept relatively stable (Figure 5E). The increased expression of the acyltransferase Are2 in the post-diauxic phase (Figures 4-B1 and 4-C3) indicates a functional role, together with Dga1 (not detected) (Kohlwein et al., 2013), in synthesizing TG. The unexpected observation that the SE level is relatively constant upon entry to the stationary phase (Figure 5E) coincides with a general down-regulation of the de novo sterol biosynthesis pathway initiated in the diauxic shift (Figure 4-C1). This finding suggests that SEs are the main source of membrane sterols as cells resume growth in the post-diauxic phase, and explains why the SE pool, unlike the TG pool, is not replenished when cells approach the stationary phase. These results are consistent with a recent study showing that the ER-associated protein degradation (ERAD) pathway down-regulates sterol biosynthesis machinery and, when defective, sustains sterol synthesis in early stationary phase cells (Foresti et al., 2013).

The above findings show independent regulation and metabolic fate of TG and SE lipids. However, not only the bulk amounts of TG and SE but also the levels of distinct TG and SE species are subject to dynamic modulation (Figures 6D and 6P). For instance, the synchronous mobilization and synthesis of abundant TG species with three MUFA moieties suggest substrate selectivity of lipases and acyltransferases in vivo (Figure 6H). In addition, the synthesis of TG species with very long chain fatty acid (VLCFA) moieties (e.g., C26:0) (Ejsing et al., 2009) is increased during the post-diauxic phase and the stationary phase (Figure 6J). As VLCFAs are typically used for ceramide synthesis, this finding suggests that lipid droplets also participate in the coordination of sphingolipid metabolism by salvaging VLCFAs that can be channeled into sphingolipid biosynthesis upon physiological demand (e.g., upon growth resumption from the stationary phase). The mobilization of TG species with VLCFA moieties has been ascribed to the lipase Tgl5 (Athenstaedt and Daum, 2005) (not detected).

Dynamics of Fatty Acid Unsaturation Correlate Protein Expression and Peroxisomal Biogenesis

We performed fuzzy c-means clustering analysis of all lipid species to delineate coordinated dynamics throughout the lipidome. This analysis revealed five clusters of lipids with distinct temporal profiles and structural signatures (Figure 7A; Table S5). Specifically, lipid species increased during the early exponential phase

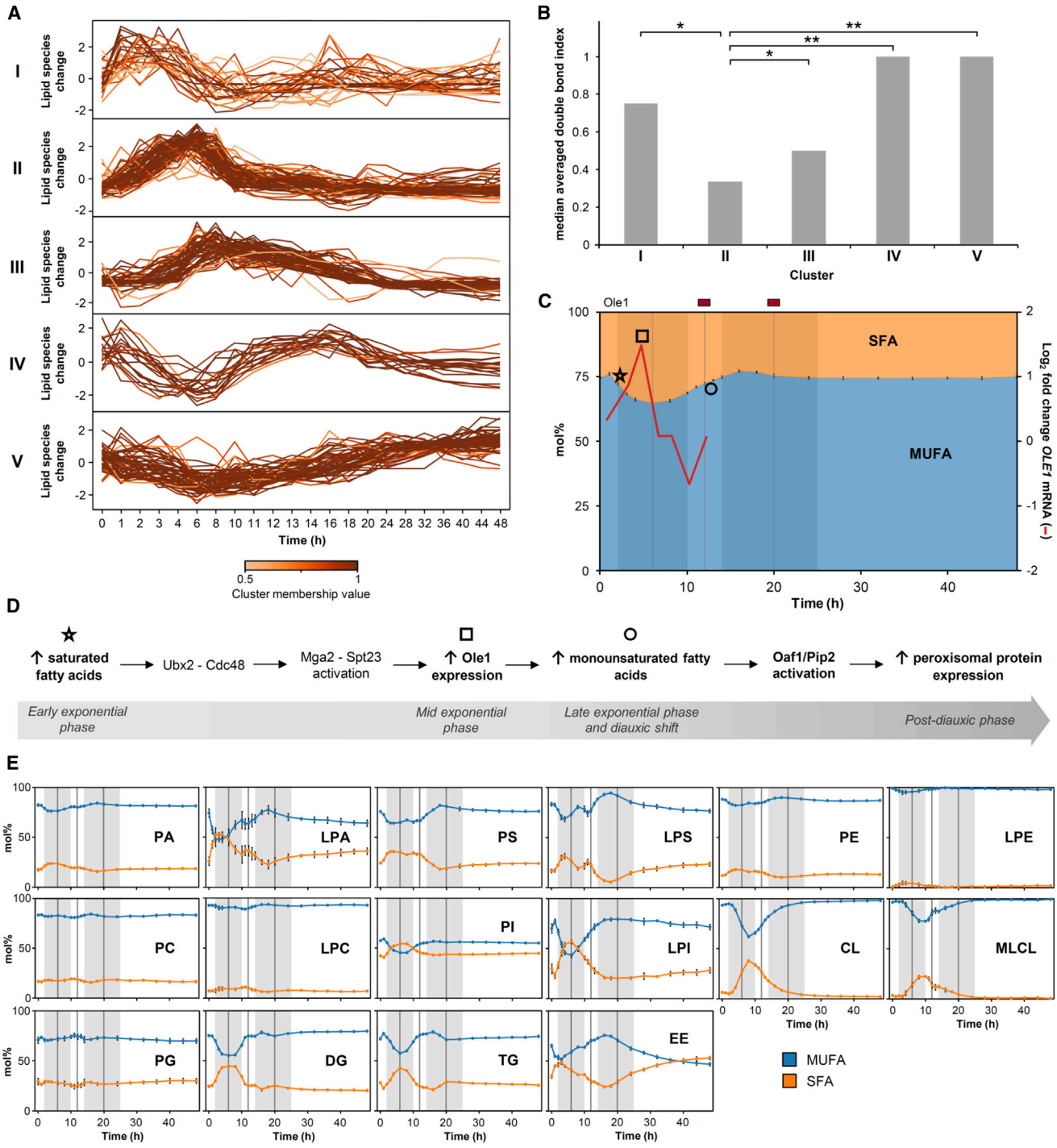

Figure 7. Modulation of Endogenous MUFA Levels Constitutes a Physiological Mechanism for Transcriptional Regulation of Protein Expression

(A) Fuzzy c-means clustering analysis of lipid species. See also Table S5.

(B) Median averaged double bond index (i.e., number of double bonds/number of fatty acid moieties in a lipid molecule) for each cluster. Statistical comparison between clusters by Wilcoxon rank-sum test. $^{*}p < 0.01$; $^{**}p < 0.001$. See also Table S5.

(C) Temporal profile of SFA and MUFA moieties in the lipidome. The relative abundance of SFA and MUFA is calculated as described in the Supplemental Experimental Procedures. The results are expressed as the mean ± SD of five biological replicates. Statistical comparisons by repeated measures ANOVA and post hoc paired *t* test (see Table S3). Fold changes (12 hr/6 hr and 20 hr/6 hr) in Ole1 levels are indicated by color (as in Figure 4) at the top. *OLE1* transcript abundance is curated from DeRisi et al. (1997) (see Supplemental Experimental Procedures). Vertical lines indicate the time points selected for proteomic analysis. Shaded areas correspond to phases of proliferation. Symbols relate to processes depicted in (D).

(legend continued on next page)

(cluster II) comprise a high proportion of saturated fatty acid (SFA) moieties, whereas lipid species increased in the late exponential phase and the diauxic shift (cluster IV) feature a high proportion of MUFA moieties (Figure 7B; Table S5). This finding was substantiated by an in silico analysis of the total complement of SFA and MUFA moieties in the lipidome, which uncovered a systematic increase in the total level of SFA moieties until the mid-exponential phase followed by an increase in the total level of MUFA moieties until the post-diauxic phase (Figure 7C).

To gain further insight into the modulation of MUFA levels, we assessed the expression level of Ole1, the only fatty acid desaturase in *S. cerevisiae*. Ole1 abundance is comparatively high at the mid-exponential phase (Figure 4-A1), coinciding with the apex of total SFA levels and the onset of the increase in MUFA levels (Figure 7C). Subsequently, Ole1 levels decrease as the levels of MUFA are restored. In addition, curated *OLE1* mRNA levels from a transcriptomic study of the diauxic shift (DeRisi et al., 1997) match these observations showing a transient increase in *OLE1* mRNA abundance as the total SFA levels reach their apex (Figure 7C). *OLE1* expression is regulated by two transcription regulators, Mga2 and Spt23, which are integral ER proteins proteolytically activated via an ubiquitin/proteasome-dependent process mediated by Ubx2 (Surma et al., 2013) and Cdc48 (Hoppe et al., 2000; Rape et al., 2001). Interestingly, Ole1 expression and activity are up-regulated by supplementation with SFAs and conversely down-regulated by MUFAs (Bossie and Martin, 1989; Choi et al., 1996), which suggests that permutations of membrane lipid composition elicit a regulatory cue via the ERAD pathway to modulate fatty acid desaturase activity (Surma et al., 2013). Our results indicate that the increased levels of endogenous SFAs can be the physiological cue for up-regulation of Ole1 expression and the increase in MUFA synthesis (Figures 7C and 7D). Interestingly, we found a non-uniform distribution of SFA and MUFA moieties throughout the lipidome, with distinct membrane lipid classes that selectively incorporate SFAs during the early exponential phase and likely contribute to the changes in membrane composition that trigger Ole1 expression (Figure 7E).

Similarly, the expression of peroxisomal proteins including the β-oxidation enzymes is induced by exogenous supplementation with MUFAs via the heterodimeric transcription factor Oaf1/Pip2 (Karpichev and Small, 1998; Phelps et al., 2006). Binding of MUFA to Oaf1 induces its translocation to the nucleus and activation of gene expression (Phelps et al., 2006). We performed a transcription factor over-representation analysis to test whether the increase in the endogenous MUFA levels (Figure 7C) participates in the transcriptional program of peroxisomal protein expression. This analysis identified transcription factors reported to be involved in the diauxic shift including the Hap2/3/4/5 complex, Msn2 and Msn4, Cat8, and Adr1 (DeRisi et al., 1997; Haurie et al., 2004) (Table S6). Moreover, Oaf1 and Pip2 are over-represented demonstrating that the Oaf1/Pip2-dependent peroxisomal protein expression occurs in vivo when MUFA levels are high. Interestingly, recent studies have shown that Oaf1 translocates to the nucleus under low glucose conditions (Karpichev et al., 2008) and that Oaf1 can regulate gene expression in the diauxic shift (Zampar et al., 2013). Our results extend these findings and indicate that modulation of endogenous MUFA levels constitutes a physiological upstream activator that regulates Oaf1/Pip2-dependent protein expression and peroxisomal biogenesis in vivo (Figure 7D).

SIGNIFICANCE

Our work presents a proteolipidomics platform for a comprehensive and quantitative time-resolved analysis of the yeast proteome and lipidome. We applied this platform to investigate to what extent lipid metabolism is regulated under changing conditions and its impact at the cellular level. Our results reveal regulation of lipid metabolism at the global scale during physiological adaptations, which challenges the traditional view and research focus on specific lipids and their individual metabolic conversions and functions. In particular, we uncover coordinated regulation of (i) glycerophospholipid metabolism to support mitochondrial function and membrane dynamics, (ii) sphingolipid metabolism in a previously unrecognized growth stage-specific manner, and (iii) mobilization and storage of lipid droplet-associated TG and SE species to sustain membrane and energy homeostasis. In addition, fluctuations of lipid species across the entire lipidome revealed that endogenous synthesis of unsaturated fatty acids constitutes an in vivo upstream activator of peroxisomal biogenesis via the heterodimeric Oaf1/Pip2 transcription factor. These findings demonstrate the central role of lipid metabolism in adaptive processes and underscore the need to investigate its regulation at the global scale to understand cell physiology. We note that the proteolipidomics platform can in future be complemented with cell fractionation strategies and quantitative assessment of post-translational modifications (e.g., protein phosphorylation) to interrogate in further detail how protein localization and signaling networks govern global lipid metabolism and cell physiology. In conclusion, our work provides a comprehensive reference of lipid and protein dynamics as a quantitative resource for future studies, and defines time-resolved quantitative systems-level analysis of lipid and protein dynamics as a new paradigm for studying the regulation and function of lipid metabolism.

EXPERIMENTAL PROCEDURES

Full methods are available in the Supplemental Experimental Procedures.

Yeast Culture Conditions and Sampling

The yeast *S. cerevisiae* (strain BY4742) was used in this study. A frozen stock was streaked on a YPD plate (1% w/v yeast extract, 2% w/v peptone, 2% w/v glucose, 2% w/v agar) and grown at 30°C for 36 hr. Yeasts were precultured at 30°C for 24 hr in YPD medium (1% w/v yeast extract, 2% w/v peptone, 2% w/v

(D) Temporal reconstruction of processes related to modulation of endogenous SFA and MUFA levels; based on the results of this study (bold), transcriptomic data (DeRisi et al., 1997), and biochemical studies (Karpichev and Small, 1998; Surma et al., 2013). See also Table S6.

(E) Lipid class-specific changes in SFA and MUFA content. The relative abundance of SFA and MUFA is calculated as described in the Supplemental Experimental Procedures. The results are expressed as the mean ± SD of five biological replicates. Vertical lines and shaded areas as in (C).

glucose). Precultured yeast cells were batch cultured in five biological replicates for 48 hr in YPD medium inoculated at a starting OD_{600} of 0.2. Growth was monitored by measuring the optical density of the cultures at 600 nm. Cells were harvested for proteomic and lipidomic analysis, frozen in liquid nitrogen and stored at −80°C. One milliliter of culture broth was also withdrawn, centrifuged, and the supernatant was stored at −80°C for glucose and ethanol determination in the medium.

Quantitative Proteomics

Yeast lysates were digested with trypsin (León et al., 2013) and 5 μg of peptides were analyzed by 2D liquid chromatography (high pH reversed phase/low pH reversed phase)-tandem mass spectrometry (high reversed phase/low reversed phase pH) using a nanoAcquity UPLC (Waters) coupled with an LTQ Orbitrap XL (Thermo Scientific) equipped with a nanoelectrospray source (Proxeon, now Thermo Scientific). Peptides were identified using MASCOT and quantified with Progenesis LC-MS (Nonlinear Dynamics Limited).

Quantitative Lipidomics

Yeast lysates were spiked with a cocktail of 20 internal lipid standards and subjected to two-step lipid extraction (Ejsing et al., 2009). Lipid extracts were dried, re-dissolved in chloroform/methanol 1:2 (v/v) and analyzed using an LTQ Orbitrap XL equipped with a robotic nanoelectrospray ionization source TriVersa NanoMate (Advion Biosciences) (Ejsing et al., 2009). Sterols were analyzed after chemical sulfation (Carvalho et al., 2012). Lipidomic data analysis was performed using ALEX software (Husen et al., 2013).

Lipid Nomenclature

Lipid species are annotated according to their sum composition (Husen et al., 2013). Glycerolipid and glycerophospholipid species are annotated as <lipid class> <sum of carbon atoms in the fatty acid moieties>:<sum of double bonds in the fatty acid moieties> (e.g., PC 32:1). Sphingolipids species are annotated as <lipid class> <sum of carbon atoms in the long chain base (LCB) and the fatty acid moiety>:<sum of double bonds in the LCB and the fatty acid moiety>;<sum of hydroxyl groups in the LCB and the fatty acid moiety> (e.g., IPC 44:0;4).

Functional Annotation of Proteins

The curated GO slim and biochemical pathway annotation of individual proteins were retrieved from the *Saccharomyces* Genome Database. The average fold change of proteins within each category was calculated to identify up- or down-regulated structural components and functional processes.

Transcription Factor Over-Representation Analysis

Transcription factors associated with the regulated proteins were determined as described by Zampar et al. (2013). A protein was considered to be regulated when the ANOVA *f* value and *t* test *p* value were <0.01. The transcription factor-target gene associations (based on direct evidence) were retrieved from the Yeastract database (Teixeira et al., 2006). The resulting *p* value indicates, for each transcription factor, the probability that the observed number of associations with the set of regulated proteins would occur by chance.

Clustering of Lipidomic Data

Fuzzy c-means clustering analysis was used to identify common trends in the abundance profile of all lipid species quantified (calculated as mol% of lipid species per lipid class). Prior to calculation of mol%, missing values were substituted by half of the minimum picomole value detected for the lipid species in the dataset. The parameters of the clustering analysis, fuzzifier and number of clusters, were set as described (Schwämmle and Jensen, 2010). Each clustered lipid species has a membership value that indicates the likelihood with which it belongs to the cluster. The averaged double bond index (i.e., no. of double bonds/no. of fatty acid moieties in a lipid molecule) was calculated to identify common structural features in lipid clusters. The Wilcoxon rank-sum test was used for statistical comparisons between clusters.

Statistical Analysis

The results are expressed as the mean ± SD of five biological replicates. The statistical analysis was carried out on ln-transformed values by repeated measures ANOVA followed by post hoc paired *t* test to compare the protein or lipid species levels between the analyzed time points, and corrected for multiple hypothesis testing by calculating *q* values (false discovery rate adjusted *p* values). Differences were considered significant when the ANOVA *f* value and *t* test *p* value were <0.05 (corresponding to a *q* value <0.05).

SUPPLEMENTAL INFORMATION

Supplemental Information includes Supplemental Discussion, Supplemental Experimental Procedures, six figures, six tables, and three files and can be found with this article online at http://dx.doi.org/10.1016/j.chembiol.2015.02.007.

AUTHOR CONTRIBUTIONS

A.C., R.R.S., O.N.J., and C.S.E. conceived and designed the study. A.C., R.R.S., and H.K.H.B. conducted the experiments. A.C., R.R.S., K.T., and C.S.E. analyzed the data. D.E.R. and J.Z. performed flux balance analysis. A.C. and C.S.E. wrote the paper. O.N.J. and C.S.E. supervised all aspects of the project.

ACKNOWLEDGMENTS

We thank Peter Husen, Martin Hermansson, and Kim Ekroos for expert advice on data processing and fruitful discussion, Kristina Egede Budtz and Peter Højrup for amino acid analysis, and Robin W. Klemm and Tobias C. Walther for critical reading of the manuscript and constructive comments. This research was supported by Lundbeckfonden (R44-A4342, R54-A5858, C.S.E.), the Danish Council for Independent Research, Natural Sciences (10-094213, A.C.; 09-072484, C.S.E.), and a Marie Curie Intra-European Fellowship (A.C.).

Received: August 13, 2014
Revised: February 20, 2015
Accepted: February 22, 2015
Published: March 19, 2015

REFERENCES

Aguilar, P.S., Frohlich, F., Rehman, M., Shales, M., Ulitsky, I., Olivera-Couto, A., Braberg, H., Shamir, R., Walter, P., Mann, M., et al. (2010). A plasma-membrane E-MAP reveals links of the eisosome with sphingolipid metabolism and endosomal trafficking. Nat. Struct. Mol. Biol. *17*, 901–908.

Athenstaedt, K., and Daum, G. (2005). Tgl4p and Tgl5p, two triacylglycerol lipases of the yeast *Saccharomyces cerevisiae* are localized to lipid particles. J. Biol. Chem. *280*, 37301–37309.

Berchtold, D., Piccolis, M., Chiaruttini, N., Riezman, I., Riezman, H., Roux, A., Walther, T.C., and Loewith, R. (2012). Plasma membrane stress induces relocalization of Slm proteins and activation of TORC2 to promote sphingolipid synthesis. Nat. Cell Biol. *14*, 542–547.

Bione, S., D'Adamo, P., Maestrini, E., Gedeon, A.K., Bolhuis, P.A., and Toniolo, D. (1996). A novel X-linked gene, G4.5. is responsible for Barth syndrome. Nat. Genet. *12*, 385–389.

Bossie, M.A., and Martin, C.E. (1989). Nutritional regulation of yeast delta-9 fatty acid desaturase activity. J. Bacteriol. *171*, 6409–6413.

Breslow, D.K., Collins, S.R., Bodenmiller, B., Aebersold, R., Simons, K., Shevchenko, A., Ejsing, C.S., and Weissman, J.S. (2010). Orm family proteins mediate sphingolipid homeostasis. Nature *463*, 1048–1053.

Buescher, J.M., Liebermeister, W., Jules, M., Uhr, M., Muntel, J., Botella, E., Hessling, B., Kleijn, R.J., Le Chat, L., Lecointe, F., et al. (2012). Global network reorganization during dynamic adaptations of *Bacillus subtilis* metabolism. Science *335*, 1099–1103.

Carvalho, M., Sampaio, J.L., Palm, W., Brankatschk, M., Eaton, S., and Shevchenko, A. (2012). Effects of diet and development on the *Drosophila* lipidome. Mol. Syst. Biol. *8*, 600.

Choi, J.Y., Stukey, J., Hwang, S.Y., and Martin, C.E. (1996). Regulatory elements that control transcription activation and unsaturated fatty acid-mediated repression of the *Saccharomyces cerevisiae* OLE1 gene. J. Biol. Chem. *271*, 3581–3589.

Coller, H.A. (2011). Cell biology. The essence of quiescence. Science *334*, 1074–1075.

Costenoble, R., Picotti, P., Reiter, L., Stallmach, R., Heinemann, M., Sauer, U., and Aebersold, R. (2011). Comprehensive quantitative analysis of central carbon and amino-acid metabolism in *Saccharomyces cerevisiae* under multiple conditions by targeted proteomics. Mol. Syst. Biol. *7*, 464.

de Godoy, L.M., Olsen, J.V., Cox, J., Nielsen, M.L., Hubner, N.C., Frohlich, F., Walther, T.C., and Mann, M. (2008). Comprehensive mass-spectrometry-based proteome quantification of haploid versus diploid yeast. Nature *455*, 1251–1254.

Dennis, E.A., Deems, R.A., Harkewicz, R., Quehenberger, O., Brown, H.A., Milne, S.B., Myers, D.S., Glass, C.K., Hardiman, G., Reichart, D., et al. (2010). A mouse macrophage lipidome. J. Biol. Chem. *285*, 39976–39985.

DeRisi, J.L., Iyer, V.R., and Brown, P.O. (1997). Exploring the metabolic and genetic control of gene expression on a genomic scale. Science *278*, 680–686.

Dickson, R.C. (2008). Thematic review series: sphingolipids. New insights into sphingolipid metabolism and function in budding yeast. J. Lipid Res. *49*, 909–921.

Domon, B., and Aebersold, R. (2010). Options and considerations when selecting a quantitative proteomics strategy. Nat. Biotechnol. *28*, 710–721.

Egner, A., Jakobs, S., and Hell, S.W. (2002). Fast 100-nm resolution three-dimensional microscope reveals structural plasticity of mitochondria in live yeast. Proc. Natl. Acad. Sci. USA *99*, 3370–3375.

Ejsing, C.S., Sampaio, J.L., Surendranath, V., Duchoslav, E., Ekroos, K., Klemm, R.W., Simons, K., and Shevchenko, A. (2009). Global analysis of the yeast lipidome by quantitative shotgun mass spectrometry. Proc. Natl. Acad. Sci. USA *106*, 2136–2141.

Fairn, G.D., Hermansson, M., Somerharju, P., and Grinstein, S. (2011). Phosphatidylserine is polarized and required for proper Cdc42 localization and for development of cell polarity. Nat. Cell Biol. *13*, 1424–1430.

Foresti, O., Ruggiano, A., Hannibal-Bach, H.K., Ejsing, C.S., and Carvalho, P. (2013). Sterol homeostasis requires regulated degradation of squalene monooxygenase by the ubiquitin ligase Doa10/Teb4. Elife *2*, e00953.

Gaspar, M.L., Hofbauer, H.F., Kohlwein, S.D., and Henry, S.A. (2011). Coordination of storage lipid synthesis and membrane biogenesis: evidence for cross-talk between triacylglycerol metabolism and phosphatidylinositol synthesis. J. Biol. Chem. *286*, 1696–1708.

Grillitsch, K., Connerth, M., Kofeler, H., Arrey, T.N., Rietschel, B., Wagner, B., Karas, M., and Daum, G. (2011). Lipid particles/droplets of the yeast *Saccharomyces cerevisiae* revisited: lipidome meets proteome. Biochim. Biophys. Acta *1811*, 1165–1176.

Gu, Z., Valianpour, F., Chen, S., Vaz, F.M., Hakkaart, G.A., Wanders, R.J., and Greenberg, M.L. (2004). Aberrant cardiolipin metabolism in the yeast taz1 mutant: a model for Barth syndrome. Mol. Microbiol. *51*, 149–158.

Hanscho, M., Ruckerbauer, D.E., Chauhan, N., Hofbauer, H.F., Krahulec, S., Nidetzky, B., Kohlwein, S.D., Zanghellini, J., and Natter, K. (2012). Nutritional requirements of the BY series of *Saccharomyces cerevisiae* strains for optimum growth. FEMS Yeast Res. *12*, 796–808.

Haurie, V., Sagliocco, F., and Boucherie, H. (2004). Dissecting regulatory networks by means of two-dimensional gel electrophoresis: application to the study of the diauxic shift in the yeast *Saccharomyces cerevisiae*. Proteomics *4*, 364–373.

Henry, S.A., Kohlwein, S.D., and Carman, G.M. (2012). Metabolism and regulation of glycerolipids in the yeast *Saccharomyces cerevisiae*. Genetics *190*, 317–349.

Hoppe, T., Matuschewski, K., Rape, M., Schlenker, S., Ulrich, H.D., and Jentsch, S. (2000). Activation of a membrane-bound transcription factor by regulated ubiquitin/proteasome-dependent processing. Cell *102*, 577–586.

Husen, P., Tarasov, K., Katafiasz, M., Sokol, E., Vogt, J., Baumgart, J., Nitsch, R., Ekroos, K., and Ejsing, C.S. (2013). Analysis of lipid experiments (ALEX): a software framework for analysis of high-resolution shotgun lipidomics data. PLoS One *8*, e79736.

Karpichev, I.V., and Small, G.M. (1998). Global regulatory functions of Oaf1p and Pip2p (Oaf2p), transcription factors that regulate genes encoding peroxisomal proteins in *Saccharomyces cerevisiae*. Mol. Cell. Biol. *18*, 6560–6570.

Karpichev, I.V., Durand-Heredia, J.M., Luo, Y., and Small, G.M. (2008). Binding characteristics and regulatory mechanisms of the transcription factors controlling oleate-responsive genes in *Saccharomyces cerevisiae*. J. Biol. Chem. *283*, 10264–10275.

Klose, C., Surma, M.A., Gerl, M.J., Meyenhofer, F., Shevchenko, A., and Simons, K. (2012). Flexibility of a eukaryotic lipidome–insights from yeast lipidomics. PLoS One *7*, e35063.

Kohlwein, S.D., Veenhuis, M., and van der Klei, I.J. (2013). Lipid droplets and peroxisomes: key players in cellular lipid homeostasis or a matter of fat–store 'em up or burn 'em down. Genetics *193*, 1–50.

Lefevre, S.D., van Roermund, C.W., Wanders, R.J., Veenhuis, M., and van der Klei, I.J. (2013). The significance of peroxisome function in chronological aging of *Saccharomyces cerevisiae*. Aging Cell *12*, 784–793.

Le Guedard, M., Bessoule, J.J., Boyer, V., Ayciriex, S., Velours, G., Kulik, W., Ejsing, C.S., Shevchenko, A., Coulon, D., Lessire, R., et al. (2009). PSI1 is responsible for the stearic acid enrichment that is characteristic of phosphatidylinositol in yeast. FEBS J. *276*, 6412–6424.

León, I.R., Schwämmle, V., Jensen, O.N., and Sprenger, R.R. (2013). Quantitative assessment of in-solution digestion efficiency identifies optimal protocols for unbiased protein analysis. Mol. Cell. Proteomics *12*, 2992–3005.

Locasale, J.W., and Cantley, L.C. (2011). Metabolic flux and the regulation of mammalian cell growth. Cell Metab. *14*, 443–451.

Mann, M., Kulak, N.A., Nagaraj, N., and Cox, J. (2013). The coming age of complete, accurate, and ubiquitous proteomes. Mol. Cell *49*, 583–590.

Marguerat, S., Schmidt, A., Codlin, S., Chen, W., Aebersold, R., and Bahler, J. (2012). Quantitative analysis of fission yeast transcriptomes and proteomes in proliferating and quiescent cells. Cell *151*, 671–683.

Neilson, K.A., Ali, N.A., Muralidharan, S., Mirzaei, M., Mariani, M., Assadourian, G., Lee, A., van Sluyter, S.C., and Haynes, P.A. (2011). Less label, more free: approaches in label-free quantitative mass spectrometry. Proteomics *11*, 535–553.

Paradies, G., Paradies, V., De Benedictis, V., Ruggiero, F.M., and Petrosillo, G. (2014). Functional role of cardiolipin in mitochondrial bioenergetics. Biochim. Biophys. Acta *1837*, 408–417.

Phelps, C., Gburcik, V., Suslova, E., Dudek, P., Forafonov, F., Bot, N., MacLean, M., Fagan, R.J., and Picard, D. (2006). Fungi and animals may share a common ancestor to nuclear receptors. Proc. Natl. Acad. Sci. USA *103*, 7077–7081.

Picotti, P., Bodenmiller, B., Mueller, L.N., Domon, B., and Aebersold, R. (2009). Full dynamic range proteome analysis of *S. cerevisiae* by targeted proteomics. Cell *138*, 795–806.

Rajakumari, S., Rajasekharan, R., and Daum, G. (2010). Triacylglycerol lipolysis is linked to sphingolipid and phospholipid metabolism of the yeast *Saccharomyces cerevisiae*. Biochim. Biophys. Acta *1801*, 1314–1322.

Rape, M., Hoppe, T., Gorr, I., Kalocay, M., Richly, H., and Jentsch, S. (2001). Mobilization of processed, membrane-tethered SPT23 transcription factor by CDC48(UFD1/NPL4), a ubiquitin-selective chaperone. Cell *107*, 667–677.

Roelants, F.M., Breslow, D.K., Muir, A., Weissman, J.S., and Thorner, J. (2011). Protein kinase Ypk1 phosphorylates regulatory proteins Orm1 and Orm2 to control sphingolipid homeostasis in *Saccharomyces cerevisiae*. Proc. Natl. Acad. Sci. USA *108*, 19222–19227.

Sabido, E., Quehenberger, O., Shen, Q., Chang, C.Y., Shah, I., Armando, A.M., Andreyev, A., Vitek, O., Dennis, E.A., and Aebersold, R. (2012). Targeted proteomics of the eicosanoid biosynthetic pathway completes an integrated genomics-proteomics-metabolomics picture of cellular metabolism. Mol. Cell. Proteomics *11*, M111.014746.

Schlame, M. (2013). Cardiolipin remodeling and the function of tafazzin. Biochim. Biophys. Acta *1831*, 582–588.

Schwämmle, V., and Jensen, O.N. (2010). A simple and fast method to determine the parameters for fuzzy c-means cluster analysis. Bioinformatics *26*, 2841–2848.

Shevchenko, A., and Simons, K. (2010). Lipidomics: coming to grips with lipid diversity. Nat. Rev. Mol. Cell Biol. *11*, 593–598.

Surma, M.A., Klose, C., Peng, D., Shales, M., Mrejen, C., Stefanko, A., Braberg, H., Gordon, D.E., Vorkel, D., Ejsing, C.S., et al. (2013). A lipid E-MAP identifies Ubx2 as a critical regulator of lipid saturation and lipid bilayer stress. Mol. Cell *51*, 519–530.

Teixeira, M.C., Monteiro, P., Jain, P., Tenreiro, S., Fernandes, A.R., Mira, N.P., Alenquer, M., Freitas, A.T., Oliveira, A.L., and Sa-Correia, I. (2006). The YEASTRACT database: a tool for the analysis of transcription regulatory associations in *Saccharomyces cerevisiae*. Nucleic Acids Res. *34*, D446–D451.

Thibault, G., Shui, G., Kim, W., McAlister, G.C., Ismail, N., Gygi, S.P., Wenk, M.R., and Ng, D.T. (2012). The membrane stress response buffers lethal effects of lipid disequilibrium by reprogramming the protein homeostasis network. Mol. Cell *48*, 16–27.

Tuller, G., Hrastnik, C., Achleitner, G., Schiefthaler, U., Klein, F., and Daum, G. (1998). YDL142c encodes cardiolipin synthase (Cls1p) and is non-essential for aerobic growth of *Saccharomyces cerevisiae*. FEBS Lett. *421*, 15–18.

van Meer, G., Voelker, D.R., and Feigenson, G.W. (2008). Membrane lipids: where they are and how they behave. Nat. Rev. Mol. Cell Biol. *9*, 112–124.

Werner-Washburne, M., Braun, E., Johnston, G.C., and Singer, R.A. (1993). Stationary phase in the yeast *Saccharomyces cerevisiae*. Microbiol. Rev. *57*, 383–401.

Wymann, M.P., and Schneiter, R. (2008). Lipid signalling in disease. Nat. Rev. Mol. Cell Biol. *9*, 162–176.

Zampar, G.G., Kummel, A., Ewald, J., Jol, S., Niebel, B., Picotti, P., Aebersold, R., Sauer, U., Zamboni, N., and Heinemann, M. (2013). Temporal system-level organization of the switch from glycolytic to gluconeogenic operation in yeast. Mol. Syst. Biol. *9*, 651.